JOURNAL OF MAGNETIC RESONANCE IMAGING 12:790–794 (2000)

Technical Note

Noninvasive In Vivo Magnetic Resonance Imaging of Injury-Induced Neointima Formation in the Carotid Artery of the Apolipoprotein-E Null Mouse

David R. Manka, MS,[1] Wesley Gilson, MS,[1] Ian Sarembock, MD,[3] Klaus Ley, MD,[1] and Stuart S. Berr, PhD[1,2]*

Mice deficient in apolipoprotein-E (apoE) experience severe hypercholesterolemia, are prone to atherosclerosis, and recently have emerged as a powerful tool in the study of plaque formation. In this study, we developed magnetic resonance (MR) imaging methods to detect the progression of atherosclerosis noninvasively in a mouse model of arterial injury. Four 14-week-old apoE-deficient mice were imaged 5 weeks after beginning an atherogenic Western diet and 4 weeks after wire denudation injury of the left common carotid artery (LCCA). Information from several images was combined into high-information content images using methods previously developed. The image resolution was 47 × 47 × 750 μm^3. We acquired T1-, T2-, and proton density (PD)-weighted images (TR/TE 650/14, 2000/60, and 2000/14 msec, respectively). Each 8-bit image was placed in a separate color channel to produce a 24-bit color image (red = T1, green = PD, and blue = T2). The composite image created contrast between different tissue types that was superior to that of any single image and revealed significant luminal narrowing of the LCCA, but not the uninjured RCCA. MR images were compared with corresponding histopathology cross sections and luminal area measurements from each method correlated(r^2 = 0.61). Atherosclerotic luminal narrowing was successfully detected through MR imaging in a mouse model of arterial injury that is small, reproduces quickly, and lends itself to genetic analysis and manipulation. J. Magn. Reson. Imaging 2000;12:790–794. © 2000 Wiley-Liss, Inc.

CARDIOVASCULAR DISEASE is our nation's leading cause of death, resulting in an average of one death every 33 seconds and costing an estimated $286,000,000,000 in 1999 in the United States (1). It is imperative to understand this disease better and to be able to assess prevention and treatment methods. Animal models provide a means to study the pathogenesis and effects of intervention in a highly controlled and reproducible fashion. Noninvasive imaging of atherosclerosis in animal models greatly decreases the number of animals needed to assess statistically significant changes, because animals can serve as their own controls in studies addressing the development of atherosclerotic lesions over time.

Atherosclerosis is a very complex disease. In vitro studies have limited utility in furthering our understanding of the disease process, as do animal models that do not closely mimic the human disease. A good deal of atherosclerosis research has been performed on primates and on low-density lipoprotein (LDL) receptor-deficient rabbits (eg, the Watanabe heritable hyperlipidemic rabbit) (2). However, rabbits tend to form simple lesions that are comprised largely of foam cells and are not representative of advanced human plaques (2).

Using an animal model that is small, reproduces quickly, and lends itself to genetic analysis would be highly desirable. Mice are a prime candidate. However, mice are resistant to the development of atherosclerosis. On low-fat diets, the plasma cholesterol levels are less than 100 mg/dl. Mild atherosclerosis has been noted in C57Bl/6J mice that have been fed diets high in fat and cholesterol. However, this model is unsatisfactory because the atherosclerotic lesions that form are small, occur only in the region of the aortic valve leaflets, and do not progress to the fibrous plaque stage (3).

In 1992, a promising mouse model was created using gene targeting in mouse embryonic stem cells (4). This mouse is deficient in apolipoprotein E (apoE), one of the proteins that coats the surface of very low, intermediate, and high-density lipoproteins (VLDL, IDL, and HDL, receptively),and chylomicrons. ApoE mediates the clearance of VLDL and IDL via LDL receptors. The lack of apoE in mice ($apoE^{-/-}$) causes elevated plasma lipid levels and hypersensitivity to changes in dietary lipid levels. For example, on a low-fat chow diet (fat 4.5% by weight, and 0.02% cholesterol), plasma cholesterol levels of 494 mg/dl were reported, compared with 60 mg/dl in control animals (4). On a Western diet (fat 21%

[1]Department of Biomedical Engineering, University of Virginia, Charlottesville, Virginia 22908.

[2]Department of Radiology, University of Virginia, Charlottesville, Virginia 22908.

[3]Department of Internal Medicine, Division of Cardiology, University of Virginia, Charlottesville, Virginia 22908.

Contract grant sponsor: NIH; Contract grant number: 1 R21 CA89633-01; Contract grant sponsors: the University of Virginia Pratt Fund and The Whitaker Foundation.

Presented at the Inflammatory Paradigms in the Vasculature Meeting, Keystone, CO, 1999.

*Address reprint requests to: S.S.B., P.O. Box 801332, Department of Radiology, MR4 Building, Room 1192, University of Virginia, Charlottesville, VA 22908.

Received March 13, 2000; Accepted June 26, 2000.

and cholesterol 0.15%), plasma cholesterol levels of 1821 mg/dl were reported, compared with 132 mg/dl in control animals (4).

The elevated plasma cholesterol levels result in atherosclerotic lesions that have a distribution, microscopic appearance, and composition strikingly similar to that observed in humans (5,6). The prevalence and size of lesions increases with age. On a low-fat chow diet, lesions in young mice were located mainly in the aortic sinus and consisted of foam cells. By 9–10 months, fibrous cap lesions covered by smooth muscle cells were present in the carotid arteries, abdominal aorta, and iliac arteries. In addition, cholesterol crystals and medial involvement were commonly found in moderate to advanced lesions. Calcification was found in some of the most advanced lesions (5). Western diet-fed mice demonstrated lesions that were more severe and more prevalent (6).

The purpose of this feasibility study was to determine whether we could achieve sufficient spatial resolution and contrast using MRI to be able to measure the size of plaques quantitatively in the carotid arteries of an apoE$^{-/-}$ mouse model. The plaque size is determined by the inner perimeter, which also defines the lumen, and the outer perimeter. There are several advantages to imaging the arterial wall. It has been shown by MRI (7) and histology (8) that the arterial wall can thicken significantly before any luminal narrowing occurs. The wall can occupy up to 40% of the combined wall/lumen volume before the lumen begins to decrease in size. This process of compensatory enlargement of the lumen means that atherosclerosis can progress significantly before angiography would be able to detect a change. Thus, imaging the arterial wall provides a means of following progression of early stages of the disease.

The use of MRI to follow the development of atherosclerosis in the aorta of a mouse model has recently been reported (9). However, the feasibility of imaging atherosclerosis has not been demonstrated. Here, we study injury-induced neointima formation in the carotid artery caused by endothelial injury because the response is similar to restenosis observed in coronary arteries after balloon angioplasty. Restenosis can be described as accelerated atherosclerosis in response to arterial injury (10). We previously found that wire denudation of the left carotid artery in apoE null mice fed a Western diet resulted in robust atherosclerotic plaque (11) similar to that observed months later in noninjured arteries (12). From this perspective, the model described here may help provide insights into the pathogenesis of restenosis.

MATERIALS AND METHODS

Mice

The apoE$^{-/-}$ mice used in this study were obtained from The Jackson Laboratory (Bar Harbor, ME). Four 14-week-old female apoE$^{-/-}$ mice were MR imaged 5 weeks after beginning an atherogenic Western diet and 4 weeks after undergoing wire denudation injury of the left common carotid artery (LCCA). The recently described mouse carotid injury model of Lindner et al (13) with minor modifications (11) was used. The mice were fed a Western atherogenic diet containing 21% fat by weight (0.15% by weight cholesterol and 19.5% by weight casein without sodium cholate) for 1 week before and 4 weeks after carotid injury.

For injury, apoE$^{-/-}$ mice were anesthetized by intraperitoneal injection with a solution composed of ketamine (80 mg/kg body weight (Ketaset; Aveco, Fort Dodge, IA) and xylazine (5 mg/kg, AnaSed; Lloyd Laboratories, Shenandoah, IA) diluted in an equal volume of 0.9% sodium chloride solution. Using a midline neck incision, the left external carotid artery (LECA) was looped proximally and tied off distally with 6-0 silk suture (Ethicon, Somerville, NJ). Additional 6-0 silk ties were looped around the common and internal carotid arteries for temporary vascular control during the procedure. A transverse arteriotomy was made in the LECA, and a 0.014-inch flexible angioplasty guidewire was introduced and passed approximately 1 cm to the aortic arch. Endothelial denudation injury of the LCCA was performed using wire withdrawal injury and three passes along the common carotid artery with a rotating motion to ensure uniform and complete endothelial denudation. Following removal of the wire, the LECA was tied off and the skin closed using two suture clips. At time of sacrifice (28 days), animals were reanesthetized; following an overdose of pentobarbital (210 mg/kg IP), a 24-gauge catheter was placed in the left ventricle and in situ perfusion fixation achieved at physiologic pressure (100 mm Hg) with phosphate-buffered paraformaldehyde (4%, 0.1 mol/L, pH 7.3). Both left and uninjured right carotid arteries were excised. Serial 5-μm sections were cut from the paraffin embedded blocks and prepared for histomorphometry.

Quantitative Histopathology

The arterial segments were sectioned transversely at 0.1–0.2-mm intervals, dehydrated in ethanol and xylene, and embedded in paraffin. Sections (5 μm thick) were stained by the Movat method (14). Histomorphometric analysis was performed by individuals blinded to treatment (injured vs. noninjured). For quantitative histopathologic comparisons, the mean of five sections was taken. The area of the lumen, internal elastic lamina (IEL), and external elastic lamina (EEL) was determined by planimetry and the lumen area, plaque area, medial area, I/M ratio, and overall vessel area were calculated as described elsewhere (15).

Magnetic Resonance Imaging

In vivo MRI of the mice was carried out on a Varian Associates (Palo Alto, CA) 4.7-T 200/400 VXR-S imaging system equipped with gradient coils capable of achieving 100 mT/m maximum gradient strength. Mice were positioned supine with their neck in a custom-built 2.5-m radiofrequency (RF) coil (RF Design Consulting, Newberry, FL). The RF coil was a Helmholtz pair designed to provide a uniform RF field and optimal reception of signal from mouse carotid arteries.

MRI sequences and parameters were set up to maximize the contrast and signal-to-noise ratio (SNR) of the

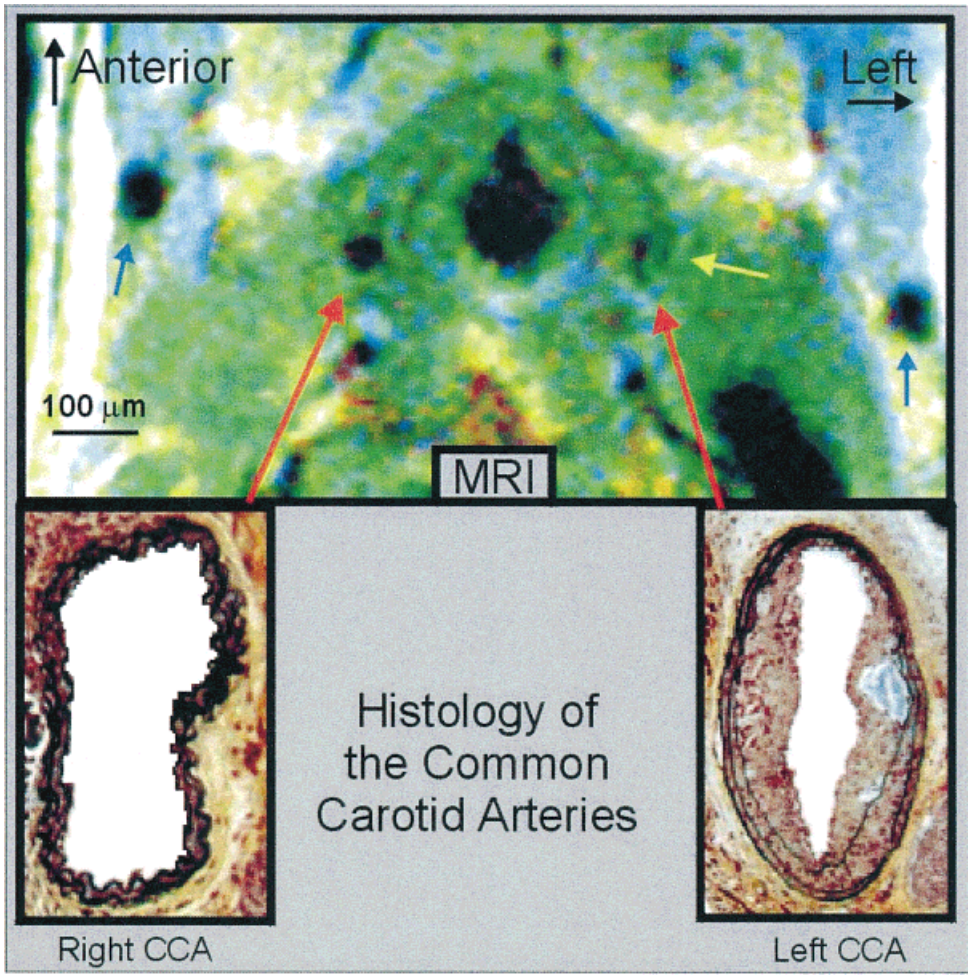

Figure 1. Top: MR composite image showing the carotid arteries of apoE$^{-/-}$ mouse 4 weeks after denudation of the left common carotid artery (LCCA). The carotid arteries are indicated by the red arrows, the jugular veins by the blue arrows, and an area of calcification/cholesterol crystals by the yellow area. Bottom: Histopathologic correlates of carotid arteries.

carotids. The slice thickness was 0.75 mm, the field of view was 2.43 × 2.43cm^2, and the matrix size was 256 × 256, zero-filled to 512 × 512, leading to a resolution of 47 × 47 × 750 μm^3. We acquired T1-, T2-, and proton density (PD)-weighted images (TR/TE = 650/14, 2000/60, and 2000/14 msec, respectively) using a multislice spin-echo sequence. Two acquisitions were used to increase SNR. The total imaging time was roughly 40 minutes. For these images, no cardiac or respiratory motion corrections were applied. To create high-contrast images, each gray-level image with T1, T2, and PD weighting was combined into a high-information content image, as described previously (7,16–18). This was done by placing each 8-bit gray-level image into a separate color channel to produce a 24-bit color image (red = T1, green = PD, and blue = T2). The composite image creates contrast between different tissue types that is superior to that of any single image. These high-information content images have been shown to provide higher contrast and a significantly greater amount of discrimination between plaque components in an image processing study of MR images of excised human aortas and carotid arteries (18). For the present study, lumen size was measured manually by three independent, blinded readers using Image Pro Plus (Media Cybernetics, Silver Springs, MD).

MR images were matched with the appropriate histology slides using the carotid bifurcation as a landmark. This matching was done by a consensus panel comprised of the three independent readers. The luminal area was calculated for both MRI and histology. These areas were tested for correlation to one another through the use of a linear regression analysis, using Sigma Stat for Windows (Jandel Scientific, San Rafael, CA). It should be noted that alignment of histology with MR images is difficult, in part due to the difference in slice thickness; The histology slices are a few microns while the MR images are several hundred. To compensate for this difference, the average from several histology slices contained within the location of a given MR imaging slice was compared with the MR image.

RESULTS

The images obtained exhibited no substantial motion artifacts. This is different from what was reported previously for mouse aorta imaging (9), where motion artifacts arose from abdominal motion due to respiration. A

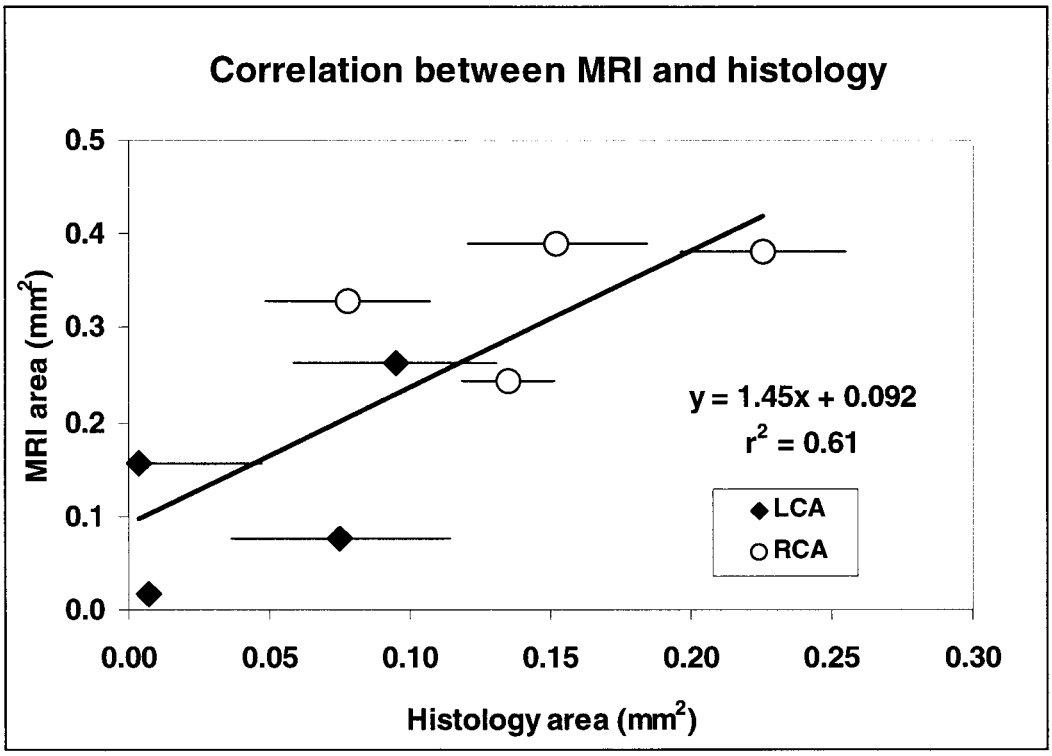

Figure 2. Correlation of histopathologic measurements with MRI measurements of carotid artery luminal areas. The closed diamonds represent the injured LCA, and the open circles represent the uninjured right carotid artery. The error bars represent the standard deviation between the measurements made from the several histology slices that corresponded to a given MRI slice. The straight line is a linear fit between the luminal areas determined by MRI and histology. There is a statistically significant correlation between the trend of the MRI measured values versus the histology-derived values.

sample MR image is presented in Fig. 1 for one of the apoE$^{-/-}$ mice. The common carotid arteries are easily identified lying to either side of the trachea and anterior to the vertebral arteries. The jugular veins (indicated by the blue arrows) are also evident. The LCCA lumen is visibly deformed, and its size is reduced due to atheromatous neointima formation following wire injury. An area of calcification/cholesterol crystals is evident in the histology and appears as a darkened area on all of the MR images (indicated by yellow arrow in Fig. 1). The RCCA appears normal on both the MR image and the histology. Neither wall thickening nor distortion of the shape or size of the RCCA lumen are evident.

While the contrast and resolution are sufficient to see areas that appear to be occupied by cholesterol crystals, the contrast and resolution were not great enough to differentiate between the tissues surrounding the artery and smooth muscle cells that had proliferated into the intima. This made it difficult to determine consistently the outer perimeter of the arterial wall and hence prevented determination of wall thickness by MRI. We could, however, measure luminal area of the common carotid arteries for both the MR images and the histology. This provided an assessment, albeit indirect, of the amount of plaque formation in the carotids. The lumen sizes determined by MRI and histology are plotted in Fig. 2. A linear correlation analysis showed a significant positive relationship between the lumen size determined by histology and MRI, respectively (n = 8, linear regression coefficient of r^2 = 0.65). The test of normality yielded P = 0.60, indicating that the source population was normally distributed about the regression line. The relationship between the lumen values determined by MRI and those determined by histology were significant (P = 0.02). The homoscedasticity test yielded P = 0.21, indicating that the variance of MRI_{lumen} was constant regardless of the value of the independent variable.

DISCUSSION

The results obtained from MRI significantly correlate with those obtained using measurements based on histologic sections. The lumen size determined by MRI was, on average, 22% greater than that determined by histology. This is consistent with the degree of shrinkage that others have found as a result of fixation of the arteries (9). It should also be noted that the slope of the fitted line shown in Fig. 2 does not pass through the origin. This suggests that a certain range of sizes of atherosclerotic lesions will be judged to be totally occluded by histology but will be partially patent, as determined by MRI. This may be in part due to fixative shrinking. It is also possible that the histology measurements underestimate the lumen size because the in vivo pressure is pulsatile and may cause a lumen size different from that observed after fixation. In addition, flow-dependent vasodilation mechanisms are likely to dilate the carotid artery in vivo, but these mechanisms are not active during fixation.

As noted by other investigators (9), differentiation of many of the atherosclerotic plaque components of interest, such as the fibrous and lipid components, is unattainable at this stage due to limited SNR and spatial resolution. Although no complete studies have been performed to characterize the lipid components of the mouse atherosclerotic plaques, it is likely that they are of similar composition to those found in humans. If this is the case, then the TE we used in this study is probably not short enough to be able to visualize short T2 lipids that are in a liquid crystalline state at body temperature. However, we were able to detect areas of darkening in the MRI that correspond to areas of calcification on the histology. This is consistent with data reported by others for the mouse abdominal aorta (9). The mouse aorta has an almost 100-fold greater cross-sectional area than the carotids (9). We may be able to improve contrast between the plaque and surrounding muscle using other types of weighting for the MR imaging such as magnetization transfer between collagen and lipoproteins, and water (17).

Our study demonstrates the feasibility of imaging the carotid arteries and documents the response to denudation injury in a mouse model relevant to the study of atherogenesis. The noninvasive methods we have developed will greatly facilitate these studies and provide information on lumen size in an animal model relevant to human atherosclerosis and restenosis in coronary arteries.

REFERENCES

1. U.S. Department of Health and Human Services, Centers for Disease Control and Prevention. Preventing cardiovascular disease: addressing the nation's leading killer, at-a-glance, 1998. http://www.cdc.gov/nccdphp/cvd/cvdaag.pdf.
2. Buja LM, Kita T, Goldstein JL, Watanabe Y, Brown MS. Cellular pathology of progressive atherosclerosis in the WHHL rabbit. An animal model of familial hypercholesterolemia. Arteriosclerosis 1983;3:87–101.
3. Paigen B. Morrow A, Brandon C, Mitchell D, Holmes P. Variation in susceptibility to atherosclerosis among inbred strains of mice. Atherosclerosis 1985;57:65–73.
4. Plump AS, Smith JD, Hayek T, et al. Severe hypercholesterolemia and atherosclerosis in apolipoprotein E-deficient mice created by homologous recombination in ES cells. Cell 1992;71:343–53.
5. Reddick RL, Zhang SH, Maeda N. Atherosclerosis in mice lacking apo E. Evaluation of lesional development and progression. Arterioscler Thromb 1994;14:141–147.
6. Nakashima Y, Plump AS, Raines EW, Breslow JL, Ross R. ApoE-deficient mice develop lesions of all phases of atherosclerosis throughout the arterial tree. Arterioscler Thromb 1994;14:133–140.
7. Merickel MB, Berr S, Spetz K, et al. Non-invasive evaluation of atherosclerosis utilizing MRI and image analysis. Arterioscler Thromb 1993;13:1180–1186.
8. Glagov S, Weisenberg E, Zarins CK, Stankunavicius R, Kolettis GJ. Compensatory enlargement of human atherosclerotic coronary arteries. N Engl J Med 1987;316:1371–1375.
9. Fayad ZA, Fallon JT, Shinnar M, et al. Noninvasive in vivo high-resolution magnetic resonance imaging of atherosclerotic lesions in genetically engineered mice. Circulation 1998;98:1541–1547.
10. Ip JH, Fuster V, Badimon L, et al. Syndromes of accelerated atherosclerosis: role of vascular injury and smooth muscle cell proliferation. J Am Coll Cardiol 1990;15:1667-1687.
11. Manka D, Wiegman P, Din S, et al. Arterial injury increases expression of inflammatory adhesion molecules in the carotid arteries of apolipoprotein-E-deficient mice. J Vasc Res 1999;36:372–378.
12. Nakashima Y, Plump AS, Raines EW, Breslow JL, Ross R. ApoE-deficient mice develop lesions of all phases of atherosclerosis throughout the arterial tree. Arterioscler Thromb 1994;14:133–140.
13. Lindner V, Fingerle J, Reidy MA. Mouse model of arterial injury. Circ Res 1993;73:792–796.
14. Movat H. Demonstration of all connective tissue elements in single section. Arch Pathol Med 1955;60:289–295.
15. Manka D, Wiegman P, Din S, et al. Arterial injury increases expression of inflammatory adhesion molecules in the carotid arteries of apolipoprotein-E -deficient mice. 1999;36:372–378.
16. Merickel MB, Carman CS, Brookeman JR, Ayers CR. Image analysis and quantification of atherosclerosis using MRI. Comput Med Imaging Graphics 1991;15:207–216.
17. Pachot-Clouard M, Vaufrey F, Darrasse L, Toussainti JF. Magnetization transfer characteristics in atherosclerotic plaque components assessed by adapted binomial preparation pulses. MAGMA 1998;7:9–15.
18. Merickel MB, Carman CS, Brookeman JR, et al. Identification and 3-D quantification of atherosclerosis using magnetic resonance imaging. Comput Biol Med 1988;18:89–102.